J Appl Physiol 94: 1213–1229, 2003.
First published December 20, 2002; 10.1152/japplphysiol.00639.2002.

Integration-differentiation and gating of carotid afferent traffic that shapes the respiratory pattern

DANIEL L. YOUNG,[1] FREDERICK L. ELDRIDGE,[2] AND CHI-SANG POON[1]
[1]*Harvard-MIT Division of Health Sciences and Technology, Massachusetts Institute of Technology, Cambridge, Massachusetts 02139; and* [2]*Department of Cell and Molecular Physiology, University of North Carolina, Chapel Hill, North Carolina 27599*

Submitted 15 July 2002; accepted in final form 15 November 2002

Young, Daniel L., Frederick L. Eldridge, and Chi-Sang Poon. Integration-differentiation and gating of carotid afferent traffic that shapes the respiratory pattern. *J Appl Physiol* 94: 1213–1229, 2003. First published December 20, 2002; 10.1152/japplphysiol.00639.2002.—The phase-dependent plasticity of carotid chemoafferent signaling was studied with electrical stimulation of a carotid sinus nerve during either inspiration or expiration in anesthetized, glomectomized, vagotomized, paralyzed, and ventilated rats. Stroboscopic and interferometric analyses of the resulting phase-contrast disturbances of the respiratory rhythm revealed that carotid chemoafferent traffic was dynamically filtered centrally by a parallel bank of leaky integrators and differentiators, each being logically gated to the inspiratory or expiratory phase in a stop-and-go manner as follows: *1*) carotid short-term potentiation of inspiratory drive was mediated by dual integrators that both shortened inspiration and augmented phrenic motor output cooperatively in long and short timescales; *2*) carotid short-term depression of respiratory frequency was mediated by a (possibly pontine) integrator that lengthened expiration with a relatively long memory; and *3*) carotid "chemoreflex" shortening of expiration was mediated by an occult fast integrator, which, together with carotid short-term depression, formed a differentiator. These effects were modulated anteriorly by integrators in the nucleus tractus solitarius that were "autogated" to, or recruited by, the carotid sinus nerve input. Such phase-selective and activity-dependent time-frequency filtering of carotid chemoafferent feedback in parallel neurological-neurodynamic central pathways may profoundly affect respiratory stability during hypoxia and sleep and could contribute to the dynamic optimization of the respiratory pattern and maintenance of homeostasis in health and in disease states.

short-term potentiation and depression; neural plasticity; respiratory stability; stroboscopic interferometric filtering technique; neural integrator and differentiator

MEMORY AND PHASE-DEPENDENT gating of afferent inputs are hallmarks of the respiratory control system (reviewed in Refs. 18, 52, 57, 61). In particular, brief hypoxia or electrical stimulation of the carotid sinus nerve (CSN) in some mammalian species induced short-term potentiation (STP) of inspiratory drive, characterized by an afterdischarge of phrenic motor activity (79), and a short-term depression (STD) of respiratory rhythm, characterized by a poststimulus decrease of respiratory frequency (6, 10, 23). Recently, it has been shown that carotid STP manifests itself not only as afterdischarge of inspiratory activity but also as sustained shortening of inspiratory duration (T_I) in the poststimulus period (59). Furthermore, both forms of STP resemble a biphasic leaky integrator (52, 59) with differing integration time constants in the induction phase and recovery phase during and after stimulation, respectively (59, 79). In contrast, recent studies showed that carotid STD of respiratory frequency stems mainly from a corresponding prolongation of expiratory duration (T_E), with induction and recovery dynamics resembling those of a biphasic leaky differentiator (58). Both carotid STP and STD are abolished or braked by pharmacological blockade of *N*-methyl-D-aspartate (NMDA) receptor channels (7, 58, 59).

These phenomena, when taken together, point to several interesting features of carotid chemoafferent signaling for respiratory pattern generation. First, the distinctive effects of carotid chemoreflex, STP, and STD on inspiratory motor output and respiratory rhythm suggest a plurality of carotid chemoafferent pathways. Among them, a critical area in the ventrolateral pons has been shown to mediate the hypoxia-induced carotid STD of respiratory frequency (10). Although the loci of carotid STP and carotid chemoreflex pathways are not clearly understood (reviewed in Ref. 57), it has been suggested that stimulation of carotid chemoreceptors may activate parallel central pathways that contribute separately to the shortening of T_I and increase of inspiratory motor output (42, 43, 71). Second, the differing effects of carotid STP and STD on T_I and T_E suggest that the corresponding pathways may be logically gated or locked to the inspiratory (I) and expiratory (E) phases of the respiratory rhythm, respectively. Third, such dynamic afferent modula-

Original submission in response to a special call for papers on "Plasticity in Respiratory Motor Control."

Address for reprint requests and other correspondence: C.-S. Poon, Harvard-MIT Division of Health Sciences & Technology, Bldg. E25–501, Massachusetts Institute of Technology, 77 Massachusetts Ave., Cambridge, MA 02139 (E-mail: cpoon@mit.edu).

The costs of publication of this article were defrayed in part by the payment of page charges. The article must therefore be hereby marked "*advertisement*" in accordance with 18 U.S.C. Section 1734 solely to indicate this fact.

tion of the respiratory rhythm, with a short-term memory that persists beyond the primary stimulus, implies that the maintenance of carotid STP and STD may involve tonic secondary inputs in convergent pathways preceding the respiratory oscillator, in addition to the primary CSN stimulus itself (57–59). Finally, the complementarities of carotid STP and STD as neural integrator and differentiator, or low-pass and high-pass filters (57, 82), with similar dependence on NMDA receptors suggest that they may spring from similar mechanisms. These observations shed light into the intricate architecture of the neural network that regulates carotid chemoafferent traffic in the brain.

To elucidate the integrative behavior of this complex neural network en bloc, we first propose a "top-down" (84) working model that consolidates the aforementioned discrete hypotheses regarding the pathway and phase specificity of carotid chemoreflex, STP, and STD. Within this conceptual framework, we introduce an advanced system identification method called "stroboscopic interferometric filtering technique" (SIFT), an analytical approach (82) employing strobe stimuli that are phase locked to a base rhythm to resolve the spatiotemporal components of afferent signaling in parallel gated or ungated pathways. With the use of this analytical procedure, we characterized the dynamic logic responses of the respiratory-pattern generator to strobe CSN inputs in anesthetized, glomectomized, vagotomized, paralyzed, and ventilated rats. The results corroborated the working model and revealed some novel features that were obscured under stepwise CSN pulse-train stimulation or hypoxic stimulation typical of previous studies. The resultant model of carotid chemoafferent signaling unifies several reported neuronal mechanisms and offers a methodical guidepost for future elucidation of other postulated elemental structures and functions at the cellular level.

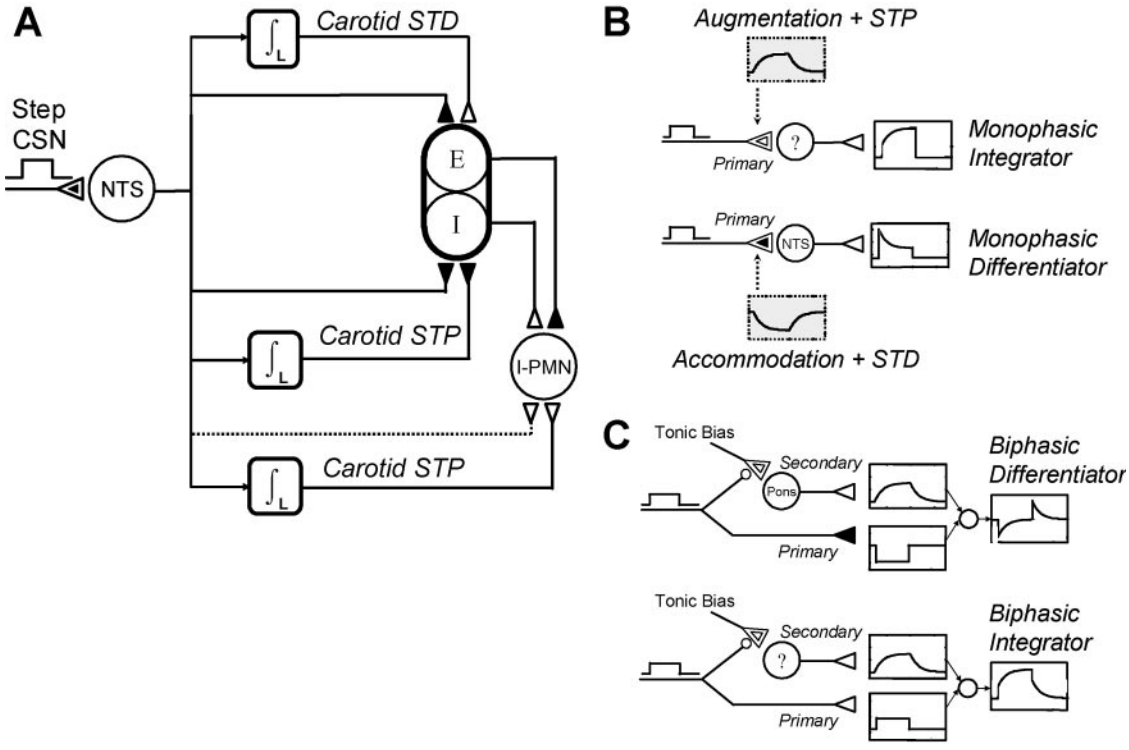

Fig. 1. *A*: working model of carotid chemoafferent processing. The respiratory oscillator is depicted as biphasic with reciprocally inhibiting expiratory (E) and inspiratory (I) aggregate superneurons that respectively inhibit (▲) and excite (△) inspiratory premotoneurons (I-PMN). Inputs from carotid sinus nerves (CSN) induce synaptic accommodation and short-term depression (STD) or long-term depression (LTD) (inner ▲) in the nucleus tractus solitarius (NTS), which signals the respiratory oscillator via parallel reflex and leaky integrator ($\int_L$) pathways. Carotid STD is mediated by an integrator pathway that promotes the E phase, whereas carotid short-term potentiation (STP) is mediated by an inhibitory integrator pathway to the I phase and an excitatory integrator pathway to I-PMN. A reflex pathway (dotted line) may also directly excite I-PMN in cat (79) and rat (23) perhaps only with relatively high-CSN stimulus amplitudes, since lower stimulation amplitudes did not elicit this reflex in the rat (59). *B*: Monophasic integrator with step (*top*) or differentiator (*bottom*) may be produced in a primary, autogated pathway such as NTS or other ("?") sites through monosynaptic STP (inner △) or STD (inner ▲) with augmentation or accommodation of synaptic transmission, respectively. Open boxes show neural activity, and shaded boxes show synaptic activity. *C*: biphasic integrator is obtained if the primary input presynaptically induces STP (double △ with ○) in a secondary pathway (such as the pons) excited by a tonic input, which sustains an "afterdischarge" after the primary input is removed. The leaky integrators depicted in *A* are of this type. Note that synaptic STD produces inverted neural integrators. A biphasic differentiator is obtained (*top*) when a biphasic integrator is combined with antagonistic reflex via the primary pathway or a biphasic integrator-with-step (*bottom*) when combined with agonist reflex.

THEORY AND METHODS

Working Model of Carotid Chemoafferent Signaling

Figure 1*A* depicts a working model of carotid STP and STD developed from previous studies with stepwise CSN pulse-train stimulation, carotid chemoreceptor stimulation, or hypoxic stimulation. The model comprises five subsystems: *1*) the respiratory oscillator, *2*) carotid chemoafferent relay neurons in the nucleus tractus solitarius (NTS), *3*) carotid chemoafferent signaling for the E phase, *4*) carotid chemoafferent signaling for the I phase, and *5*) inspiratory premotoneurons (I-PMN).

Respiratory oscillator. Previous models of carotid chemoreflex (1, 9, 22, 28) have assumed a black-box representation of the respiratory oscillator and its afferent and efferent processes. These system-level functional models adequately describe the ventilatory responses to hypoxic and hypercapnic inputs but not the corresponding changes in respiratory pattern. In contrast, recent models of the respiratory oscillator (14, 43, 65–67, 77) have postulated various neural network configurations for the sundry respiratory neurons that are thought to contribute to respiratory pattern generation. However, although these sophisticated models are capable of simulating the three-phase respiratory pattern, none of them has satisfactorily reproduced the effects of respiratory afferent inputs, such as the carotid chemoreflex response. Moreover, none of the proposed neural network configurations has been fully validated experimentally to the exclusion of other competing models, and the precise interneuronal and afferent-efferent connectivities of the respiratory oscillator remain largely uncertain.

Because the focus of the present study was the effects of carotid STP and STD on T_I, T_E, and phrenic activity rather than the neurogenesis of the three-phase respiratory pattern per se, it suffices to represent the respiratory oscillator as a half-center oscillator (37, 76), which requires minimal assumptions about the underlying neuronal connectivity. In this rendering of the respiratory oscillator, the I and E "neurons" are aggregate superneurons that are reciprocally inhibited, with T_I and T_E being determined by the balance of the phasic and tonic excitation and inhibition on both. Structurally, each superneuron may be viewed as a conglomerate of several subtypes of I- or E-related neurons in the ventral respiratory group (VRG), whereas functionally, each superneuron encapsulates the emergent properties of these neurons for setting T_I and T_E without regard to their specific temporal firing patterns, which are nonessential for the present purpose. It has been shown (37) that the I and E phases of such a half-center model display similar nonlinear interactions with afferent inputs as with a three-phase respiratory network, suggesting that the collective behavior of the varied I- and E-related neuronal subtypes in setting the respiratory rhythm is adequately described by their overall reciprocal inhibition.

In addition, previous studies (37) have shown that, for sustained oscillation to occur, both the I- and E-neuron should receive balanced tonic excitation (presumably from the central chemoreceptors), and at least one of them should exhibit spike frequency adaptation (presumably due to calcium-activated potassium currents). For simplicity, these implicit features are not depicted in Fig. 1*A*.

NTS relay. The CSN-mediated inputs from carotid chemoreceptors are relayed centrally by glutamatergic neurons in the NTS (21, 69). These neurons are known to exhibit activity-dependent synaptic accommodation (33, 40, 41, 85, 86), characterized by a gradual decrease of synaptic strength at a rate and magnitude proportionate to the frequency of repetitive afferent stimulation, which persists as STD poststimulation (type I behavior). Some first-order excitatory synapses in the NTS also exhibit NMDA-receptor-dependent long-term depression (LTD) on repetitive low-frequency (60, 85) or high-frequency (54) afferent stimulation (type II behavior). Presently, it is not clear whether carotid chemoafferent relay neurons in NTS are type I or type II neurons. We hypothesize that carotid chemoafferent relay neurons in the NTS signal the respiratory oscillator via multiple parallel pathways that separately control T_E and T_I with distinct expressions of carotid STD and STP. For simplicity, the possible influence of other descending or ascending inputs convergent to NTS neurons (20, 46, 48, 68, 74, 78, 81) is excluded in this model.

Carotid signaling for E phase. Carotid STD is modeled as a leaky neural integrator that promotes the E phase (58), presumably by excitation of E-neuron (or inhibition of I-neuron) via the ventrolateral pontine pathway (6, 10). The putative carotid chemoreflex shortening of T_E is tentatively assumed to be mediated by an inhibitory primary pathway (4, 5, 8), which combines with the parallel carotid STD pathway to form a biphasic differentiator that is gated to the E phase (58). These agonist-antagonist pathways with differing response dynamics may account for the absence of net changes in T_E on sustained carotid chemoreceptor activation (72) and the presence of posthypoxic frequency depression (6, 10).

Carotid signaling for I phase. Carotid STP is modeled as leaky neural integrators for the I phase (59), which secondarily promote ventilatory output presumably through parallel excitation of I-PMN and inhibition of I-neuron (or excitation of E-neuron). In addition, direct excitation and inhibition of these neurons via corresponding primary pathways (31, 42) may account for the carotid chemoreflex augmentation of inspiratory motor output and shortening of T_I, respectively. These parallel integrator and reflex pathways are assumed to be gated to the I phase independently of those for the E phase, which have distinct response dynamics (see Figs. 4 and 5).

Carotid signaling for I-PMN. The bulbospinal I-PMNs in dogs have been shown (11, 30, 39) to receive tonic and phasic excitatory inputs that are dependent on NMDA and α-amino-3-hydroxy-5-methyl-4-isoxazolepropionic acid receptors, respectively, as well as phasic inhibitory inputs that are dependent on both type A γ-amino-butyric acid ($GABA_A$) and glycine receptors. These observations are captured in the present I-PMN model with a tonic CSN input featuring NMDA receptor-dependent STP (59) as well as phasic excitation and inhibition from I- and E-neuron, respectively. This model is supported by recent spike train cross-correlation analyses in cats and rats that suggested that I-PMN receives tonic excitation from carotid chemoreceptor inputs (42) as well as phasic excitation (42) and phasic inhibition (14) from I-related and E-related neurons in the VRG, respectively. Presumably, the tonic and phasic excitations determine the gain and the pattern of the inspiratory drive, respectively, whereas the phasic inhibition provides the gating.

Models of Neural Integrator and Differentiator

Monophasic integrator and differentiator. The neural integrator and differentiator characterizations of carotid STP and STD (52, 58, 59) conform to a class of neural networks capable of "brain calculus" operations (38, 57). The mechanisms of such sophisticated neural computations are presently unclear; for neural integrator characterization, the candidate hypotheses include reverberation in a recurrent

network (18, 64) and activity-dependent phasic augmentation of excitatory synaptic transmission with poststimulus STP (59, 73, 79). However, the feasibility of a reverberating integrator network has been questioned on theoretical grounds due to its inherent complexity and nonrobustness to instability (82). Indeed, extensive experimental explorations have failed to confirm reverberation as a cause of respiratory afterdischarge (79), whose demonstrated dependence on NMDA receptor (59) suggests a possible involvement of glutamatergic excitatory synapses. These observations lend support for synaptic augmentation-STP as a possible cellular correlate of neural integrator (Fig. 1, *B* and *C*).

For carotid STP, the synaptic augmentation-STP hypothesis is bolstered by the established prevalence of phasic synaptic accommodation in NTS neurons (33, 40, 41, 85, 86), which is accompanied by poststimulus STD or LTD (60, 85, 86). The accommodation-STD adaptation characteristic is functionally equivalent to an inverted integrator, i.e., a neural integrator with reverse polarity. Combination of such an inverted integrator with the primary reflex leads to a neural differentiator (82) (Fig. 1*B*). From a behavioral perspective, integrator effects conform with the sensitization of a primary or secondary stimulus, whereas inverted integrator or differentiator effects conform with the habituation of a primary stimulus or desensitization of a secondary stimulus (75, 82).

An important yet subtle implication of the monosynaptic STP/STD hypothesis is that such an integrator/differentiator is necessarily monophasic, and poststimulus memory is not sustained (Fig. 1*B*). This is because of an intrinsic "autogating" of primary afferent pathways (82), namely, an abrupt silencing of neurotransmission once the primary stimulus ceases. For CSN inputs, this autogating of the first-order synapse in the NTS is not affected by spontaneous firing in second-order or higher order NTS neurons but may be obviated by tonic activity of the carotid chemoreceptors. Because the latter is precluded by CSN transection, the autogating effect is most pronounced in studies with electrical stimulation of a severed CSN.

Biphasic integrator and differentiator. Another way to sustain poststimulus memory is through a tonic secondary input (possibly from central chemoreceptors) in a convergent pathway (Fig. 1*C*), with synaptic STP/STD being induced pre- or heterosynaptically in the secondary pathway or homosynaptically in the common pathway following the confluence of the primary and secondary pathways (58). In the heterosynaptic and homosynaptic configurations, the STP/STD effect is necessarily accompanied by a reflex response (a stepwise response at the beginning and end of the CSN input) mediated by the primary pathway (see Fig. 1*B*). In the presynaptic configuration, where the CSN input serves only a modulatory role, a reflex effect is absent unless there is a bypass pathway (Fig. 1*C*). Such agonistic and antagonistic combinations of reflex (primary) and integrator (secondary) pathways with resultant integrator-plus-reflex (integrator-with-step) and differentiator effects are hypothesized in the working model for carotid STP and STD (Fig. 1*A*).

Polarity of integrator in relation to signaling pathway. In Fig. 1*A*, the presumed polarity of an integrator is related to that of the corresponding pathway relative to the respiratory rhythm. For example, the pontine integrator may be either normal or inverted (with corresponding synaptic STP or STD) depending on whether the carotid STD pathway is excitatory or inhibitory to E-neuron (or alternatively, inhibitory or excitatory to I-neuron). Thus the carotid STD prolongation of T_E may result from either increased excitation or decreased inhibition of E-neuron (alternatively, either increased inhibition or decreased excitation of I-neuron) by the pontine pathway. Such an interrelationship between the polarity of a neurotransmission pathway and of its neural plasticity is characteristic of feedforward neural networks organization (56).

Stroboscopic Interferometric Filtering Technique

From Fig. 1, it can be seen that abrupt application of carotid chemoafferent input may elicit a multiplicity of reflex, accommodative, memory, and gating effects in the NTS and the secondary pathways, which cannot be resolved readily. Although the reflex and memory components may be dissociated to some extent by phasic stimulation in alternate breath cycles or half-cycles (15, 26, 35, 36, 79), the resultant effects remain rather complex and difficult to decipher.

To circumvent this difficulty, we introduce a novel system identification procedure (82) called SIFT by analogy to stroboscopy and interferometry, two established techniques for studying phasic phenomena. Here, phasic CSN stimuli are synchronized to either the respiratory E or I phase in a stroboscopic fashion. The resulting phase-contrast input-output relationship serves both as a "stroboscope" that distinguishes the phasic (reflex or accommodative) and memory effects and as an "interferometer" that identifies any phasic gating effects. The following stroboscopic and interferometric principles for strobe CSN inputs can help to "sift" the resultant respiratory response into corresponding reflex, memory, and gating components in varying carotid chemoafferent signaling pathways.

On-strobe filtering of synaptic transmission in NTS. The synaptic accommodation and STD/LTD components of NTS neurons (60, 85) may be discriminated stroboscopically as follows. Specifically, synaptic accommodation modulates the reflex response to a strobe CSN input in an identical manner from strobe to strobe (Fig. 2*A*). If the latter is 1:1 phase locked to the respiratory rhythm, then the reflex and accommodation components are intertwined in the resultant response and are not distinguishable. In contrast, the synaptic STD/LTD component may accumulate exponentially with repeated strobes, resulting in a monophasic inverted integrator (and a monophasic differentiator when combined with the reflex-accommodation component) at on-strobe intervals (Fig. 2*B*). This on-strobe filtering effect obviates the confounding influence of synaptic accommodation and tags the STD/LTD and other memory components in NTS for further analysis.

Off-strobe filtering of NTS signaling. With strobe CSN inputs, the monophasic differentiator response of NTS is disabled at off-strobe intervals due to autogating. This off-strobe filtering effect (Fig. 2*B*) is specific to primary pathways and may be obscured by successive integration of the monophasic differentiator response in secondary pathways, which are not subject to autogating. Thus the off-strobe filtering effect is observable at the output only in the absence of secondary pathways.

Half-wave interference of respiratory rhythm. Because of autogating, a primary pathway may influence the respiratory rhythm only during the strobe period. The resultant response may be either a phase prolongation or phase shortening, depending on the respiratory phase relationship of the strobe input as well as the polarity (i.e., E or I promoting) of the primary pathway (Fig. 3*A*). Specifically, the primary input may excite or inhibit an oscillator neuron native to (i.e., with direct projection from) the primary pathway in or out of synchrony, eliciting, respectively, a direct response in the native neuron or crossover (inverse) response in the complementary oscillator neuron through reciprocal inhibition. A

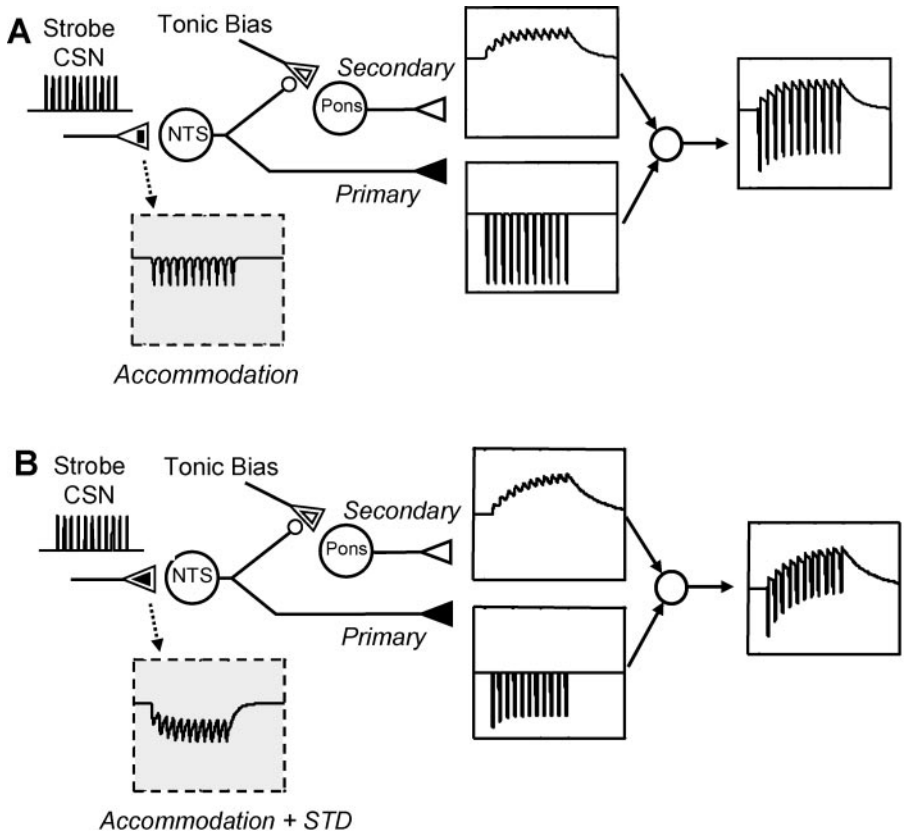

Fig. 2. Stroboscopic filtering effects due to autogating in primary pathways. Stimulus strobes (*inset* at *left*; compare with Fig. 1) in the form of repetitive CSN pulse trains are applied periodically in synchrony with the respiratory phases. Open boxes show neural activity, and shaded boxes show synaptic activity. *A*: in the absence of synaptic STD or LTD, on-strobe filtering of synaptic accommodation (■ inside triangle) in NTS leaves the primary pathway nonadaptive from strobe to strobe. *B*: off-strobe filtering of synaptic accommodation with STD or LTD (inner ▲) in NTS distinguishes the integrator effects in the primary pathway from those in the secondary pathways. This off-strobe filtering effect is specific to the primary pathway and is obscured by successive integration in the secondary pathway, which is not subject to autogating. In both examples, responses in primary or secondary pathways combine at output neuron to form a differentiator at on-strobe intervals and integrator at off-strobe intervals, with first-order dynamics in *A* and second-order dynamics in *B*.

well-known example of such native vs. crossover response patterns is the Hering-Breuer inflation reflex, in which a sustained input from pulmonary slowly adapting stretch receptors may either prolong the E phase or shorten the I phase, depending on the respiratory phase in which the input is applied (82). The magnitudes of these facilitatory or inhibitory responses are modulated by synaptic plasticity as reflected by the memory in the primary pathway, subject to the on-strobe and off-strobe filtering effects (Fig. 2). These predicted half-wave interference patterns under strobe CSN inputs serve as physiological markers for the reflex and memory effects of the primary pathway.

Full-wave interference of respiratory rhythm. In contrast, a tonic input in a primary or secondary pathway may elicit full-wave interference of the respiratory rhythm, with alternating half-cycles of native and crossover responses (Fig. 3*B*, *left*). In SIFT, the use of strobe CSN inputs predisposes the primary pathways to half-wave interference, and thus any full-wave interference patterns may serve as physiological markers for the secondary pathways.

Phase-selective filtering of carotid afferent traffic. In addition to strobe-dependent autogating of the NTS relay, carotid chemoafferent pathways may also be subject to intrinsic logic gating that is phase locked to the respiratory rhythm. For example, the full-wave interference by a tonic secondary input (Fig. 3*B*, *left*) may be rectified to half wave if the secondary pathway is logically gated to only one phase (Fig. 3*B*, *right*). This phase-selective half-wave interference, however, is not contingent on the strobe CSN inputs, and thus the effects of phase-logic gating and autogating may be readily distinguished by using strobe inputs with differing phase relationships to the respiratory rhythm.

Such phase-logic gating may also occur in the primary pathways. In this event, phase-logic gating and autogating form a logic "AND" gate in a primary pathway, i.e., the latter is active only when both gates are on.

Experimental Design and Model Testing

Based on the above SIFT theory, we tested the working model (Fig. 1*A*) experimentally by using strobe CSN inputs that were synchronized to either the I phase (SI stimuli) or E phase (SE stimuli) in anesthetized, glomectomized, and vagotomized rats. Figure 4 illustrates the varying model-predicted phase-contrast interference patterns for TE and TI mediated by the primary and secondary pathways in response to step (tonic), SI, or SE CSN inputs. For simplicity, the accommodation and STD/LTD effects in NTS are not shown. In Fig. 4*A*, the two primary pathways to the E and I neurons are seen to elicit either full-wave or half-wave modulation of TE and TI, depending on whether the CSN input is tonic or stroboscopic, respectively. In contrast, the carotid STD and STP pathways elicit only full-wave interference (Fig. 4*B*). The combined effects of the primary and secondary pathways demonstrate a mixture of half-wave and full-wave interference patterns that are characteristic of these pathways (Fig. 4*C*).

In all cases, if the signaling pathways are not phasically gated, then a response in TE elicited by a tonic input to E-neuron may echo as a crossover (inverse) response in I-neuron, and vice versa, resulting in mixed (native and crossover) disturbances in TE and TI that are correlated with one another. In contrast, if all the pathways are logically gated to the E or I phase, then the TE and TI responses to these tonic inputs become uncorrelated. It is of interest to note that, for both gated and ungated cases, the interference effects mediated by the primary pathways are always distinct for tonic and strobe CSN inputs (Fig. 4*A*), whereas those

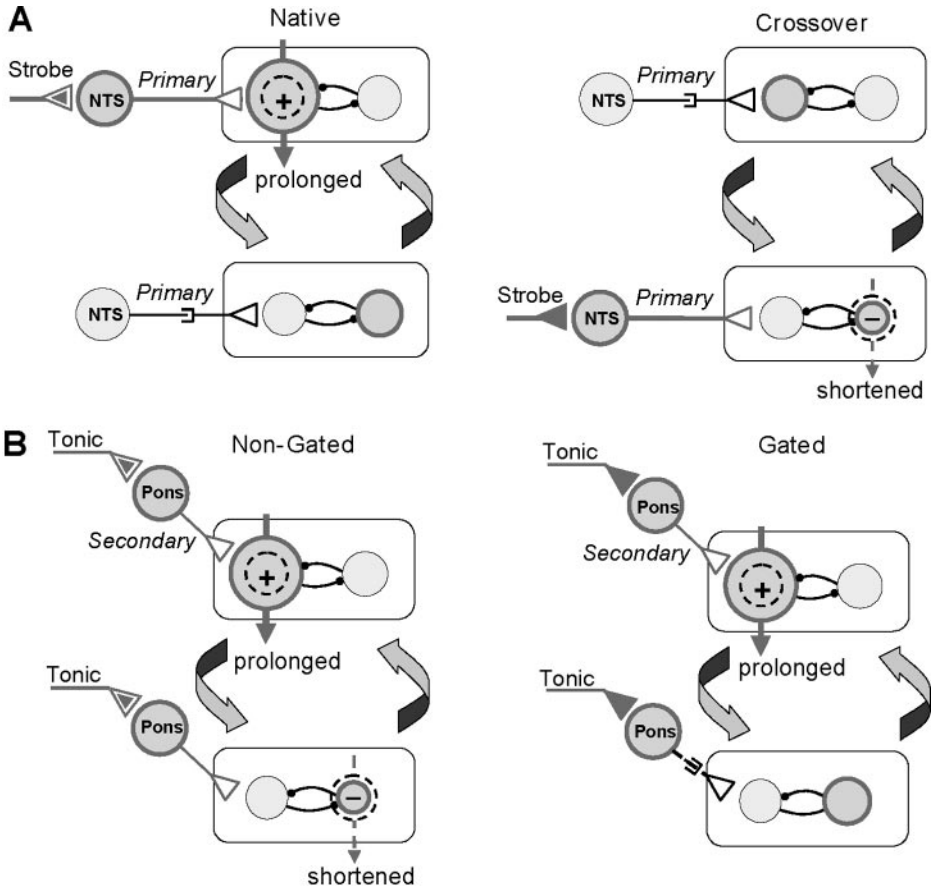

Fig. 3. Stroboscopic interference in a half-center neural oscillator. Stylized phase-transition diagrams showing oscillation between 2 reciprocally inhibiting neurons with alternating (indicated by wide curved arrows) active (dark gray) and inhibited (light gray) states. Constructive (+) and destructive interference (−) characterized by phase prolongation and shortening, respectively, are indicated by increases and decreases of neuronal sizes (denoted by bold circle with arrow) relative to control (dashed circle). *A*: half-wave interference elicited by excitatory stroboscopic input in the primary pathway (with NTS). The effect can be either + (*left*) or − (*right*) when the strobe is on and is null when strobe is off (autogating effect). *B*: full-wave interference by excitatory tonic input in the secondary pathway (with Pons) is characterized by alternating +/− half-cycles, provided that the secondary pathway is not phase-logic gated (*left*). This full-wave interference pattern may be rectified to half-wave if the secondary stimulus is logically gated to one phase (*right*). Such half-wave interference may be + (*right*) or − (not shown) depending on the phase relationship of gating. In *A* and *B*, opposite interference patterns result for inhibitory strobe or inhibitory tonic inputs (not shown).

via the secondary pathways are always qualitatively similar (Fig. 4*B*).

In preliminary model testing, we found that the reported effects of step CSN inputs on T_E and T_I (Fig. 5) and phrenic activity were satisfactorily reproduced by the working model, provided that the primary and secondary pathways were phase-logic gated (compare with Fig. 4*C*). Accordingly, SIFT analysis would predict that the T_E and T_I responses to S_I and S_E CSN inputs should display gated integrator-differentiator characteristics (Fig. 4*C*) on subtraction of the accommodation and STD/LTD effects of the NTS with on-strobe and off-strobe filtering (Fig. 2).

On the other hand, close examination of the previous step CSN data revealed that the immediate response to step application or removal of CSN input might consist of fast integrator transients that developed progressively in one or two breaths rather than abruptly in the first breath in a stepwise fashion (Fig. 5). This observation suggests the possibility that even the "reflex" response to CSN inputs might be mediated indirectly by secondary pathways with fast integrator dynamics rather than directly by primary pathways. In this event, the predicted responses to S_I and S_E CSN inputs would share certain characteristics of both models illustrated in Fig. 4, *B* and *C*. The following experiments were designed expressly to test these model predictions.

Experimental Methods

The experiments were performed on urethane-anesthetized (1.5 g/kg ip supplemented periodically at ~0.2 g/kg iv), paralyzed (pancuronium bromide, 1 mg/kg iv supplemented hourly at half initial dosage), bilaterally vagotomized, and mechanically ventilated Sprague-Dawley rats (280–400 kg; Charles River Laboratories, Wilmington, MA). For CSN stimulation, the ventilation rate was continually adjusted by the servoventilator (AVS-1 from CWE) to maintain the end-tidal CO_2 constant at a level 1–5 Torr above the apneic threshold as measured by an infrared CO_2 analyzer (Capstar-100 from CWE). A temperature-controlled heating pad (TC-831 from CWE) was used to regulate the rectal temperature at 37.5 ± 0.2°C.

A phrenic nerve (Phr) was dissected at the C_5 level via a ventral approach and mounted on custom-made silver-wire bipolar recording electrodes (OD = 0.0045 in.). Phrenic activity was amplified and low-pass filtered (AI 402 × 50, CyberAmp 380, Axon Instruments), and the resulting raw signal was time averaged with a leaky integrator (Paynter filter, time constant of ~15 ms). Both the raw Phr activity and integrated Phr activity (∫Phr) were monitored on a Tektronix digital oscilloscope and recorded (AT-MIO-16E-1, National Instruments) on a computer. The peak amplitude of ∫Phr and the phrenic burst frequency (f) were calculated for each respiratory cycle. To calculate T_I and T_E, the start of T_I (end of T_E) was defined as the point at which ∫Phr started to rise, whereas the end of T_I (beginning of T_E) was defined as the point where the slope of ∫Phr was most negative.

Both CSNs were surgically isolated and cut distally, with the adjoining tissues of one CSN (~3 mm) being removed as much as possible and away from the stimulating electrode to minimize current spread. Brief 5-s CSN stimulations (20–25 Hz, 0.1-ms pulse duration) at varying current intensities were initially used to determine the threshold current required to induce appreciable increases in phrenic activity. A

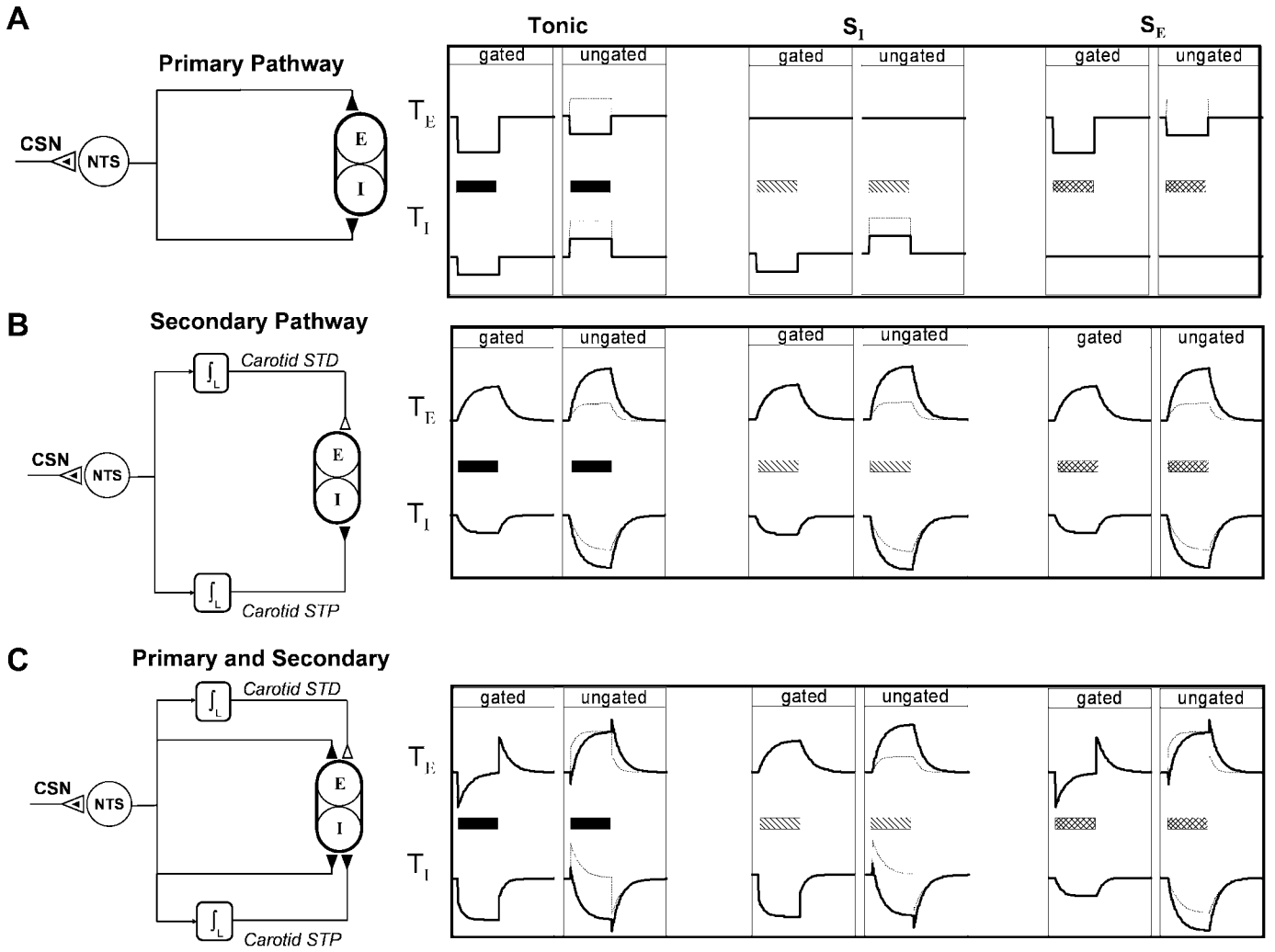

Fig. 4. Model predictions of changes in expiratory and inspiratory durations (TE and TI, respectively) in response to various CSN inputs. *Left*: special cases of the working model in Fig. 1*A*. *Right*: corresponding predicted responses to step (tonic) CSN input and inspiratory-strobe (SI) or expiratory-strobe (SE) CSN inputs, with or without phase-logic gating. Horizontal bars indicate the duration of tonic (solid bars), SI (hatched bars), or SE (crosshatched bars) CSN stimulation. Adaptations in NTS are not shown. *A*: if only primary pathways are present, step (tonic) CSN input should shorten both TE and TI independently, provided that each primary pathway is phase-logic gated to the corresponding native neuron. Otherwise, crossover responses (dotted lines) may counter or even reverse the native effects on TE and TI. SI and SE inputs produce only in-phase responses due to autogating, which may be further modulated by phase-logic gating (if present). *B*: if only secondary pathways are present, step or SI and SE CSN inputs should yield similar response patterns. For the gated case, all inputs produce progressive prolongation and shortening of TE and TI, respectively. For the ungated case, crossover effects increase the magnitudes of the corresponding gated responses. *C*: if both primary and secondary pathways are present, the response patterns are the sum of the corresponding responses in *A* and *B*.

moderate stimulus intensity (1.5–2 × threshold, 20–90 μA) was then chosen to produce increases in phrenic activity while obviating response saturation, nerve fatigue, or activation of nonmyelinated C fibers (12). At the conclusion of the experiment, the proximal CSN end was crushed, and the CSN was again stimulated to check possible current spread to the glossopharyngeal nerve. None of the animals tested showed any inhibitory or apneic respiratory response that would indicate current spread.

Electrical CSN stimuli at the chosen settings were applied stroboscopically (Fig. 6) during either the I phase (SI stimuli) or E phase (SE stimuli) over a 4-min period, which ensured that near steady-state conditions were attained in each trial for all animals. The CSN input was triggered cycle-by-cycle by using a custom-designed data-acquisition routine (LabVIEW 4, National Instruments) that detected the rising or falling edges of the ∫Phr signal. To ensure robust triggering, SI generally began within the first one-eighth to one-fourth of the rising phase, whereas SE generally began after one-half of the falling phase elapsed or after the inflection point of the declining waveform occurred. As a precaution, the SI train duration (0.15–0.25 s) and the SE train duration (0.4–0.7 s) were chosen to be always shorter than the stimulated TI and TE, respectively.

The dynamic responses were analyzed using exponential least-squares regression, and the goodness-of-fits of different

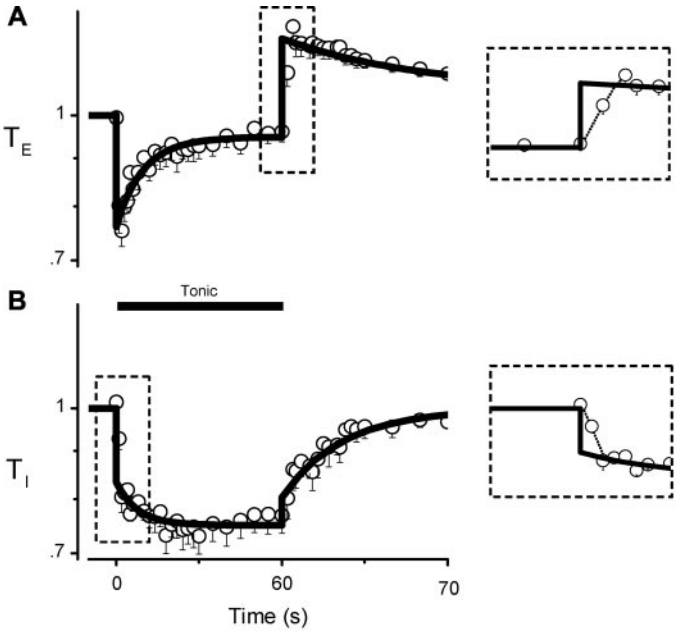

Fig. 5. Changes in phrenic burst rhythm on stepwise (tonic) CSN pulse-train stimulation in anesthetized and vagotomized rats. Data are mean values (○) of breath-by-breath TE (n = 10) and TI (n = 10) normalized to control values. Solid lines are curve fits by the working model (compare with Fig. 4*C*). Note the differentiator effects for TE with distinct time constants (onset of 10.4 ± 1.9 s; offset of 39.2 ± 18.4 s) and integrator-with-step effects for TI (onset of 5.3 ± 1.7 s; offset of 23.7 ± 3.1 s). *Insets*: enlarged views of the sections enclosed by dashed lines showing that the "reflex" components for both TE and TI responses might have developed progressively in the first 2 breaths at the onset and offset of the CSN input rather than abruptly (solid lines) in the first breath as presumed previously. These fast transient responses (dotted lines) to step CSN inputs were fitted more closely by a refined model shown in Fig. 8, which was confirmed by the present experimental study using strobe inputs. This figure was adapted from data in Refs. 58 and 59.

exponential curves were compared using the F test at the 5% significance level. Statistical significance of the parameter estimates was established using paired, two-tailed Student's t-test at the 5% level.

RESULTS

Experimental Results

Plasticity of phrenic wave shape. SI and SE CSN stimulations elicited similar time-dependent disturbances in the phrenic neurogram throughout the strobe-stimulation and recovery periods (Fig. 6*A*). In the steady state (Fig. 6*B*), SI and SE both resulted in an increase in the rate of rise of Phr activity characterized by a simultaneous increase in ∫Phr and decrease in TI, without any appreciable changes in the waveshape of ∫Phr when normalized.

Figure 7 shows the responses in TE, TI, and ∫Phr during and after SI or SE CSN stimulations observed experimentally and as fitted by multiexponential nonlinear regression. The corresponding integrator time constants and magnitudes (Table 1) are generally different from those obtained from step CSN stimulation (see Fig. 5 legend) because of the differences in the mode of activation. Some key features of the response characteristics are presented below.

Plasticity of TE. SI and SE CSN stimulations produced similar biphasic leaky differentiator-like responses in TE, with larger magnitudes for SE than for SI (Fig. 7*A*). The decrease of TE at the start of SI and SE CSN stimulations had a small but nonzero (τ_1 = 1.5–2.1 s) integrator time constant (τ), with TE reaching a nadir within the first few breaths before returning biexponentially (τ_2 = 6.5–7.8 s, τ_3 = 65–80 s) to the baseline toward the end of the strobe-stimulation period. After removal of the stimulus, TE rebounded rapidly to a peak value above the baseline, again with a small but nonzero (τ_1 = 2.4–2.9 s) integrator time constant. Thereafter, this "aftercharge" in TE gradually returned to baseline with a single slow time constant (τ_2 = 132–207 s). These SIFT response patterns for TE are similar to those resulting from step CSN inputs (58) except a reflex component was absent and replaced by a fast biphasic integrator component, and a slow monophasic integrator component was also detected.

Plasticity of TI. SI and SE CSN stimulations both produced biphasic inverted leaky integrator-like responses in TI (Fig. 7*B*) with similar response time constants and steady-state magnitudes (Table 1). Poststimulation, TI gradually returned to the baseline in the form of a biexponential afterdischarge, unlike the monoexponential decrementing response at strobe-stimulation onset. Curve fitting revealed that both the onset and offset responses had a relatively fast time constant (τ_1 = 4.9–6.9 s), whereas only the offset response had an additional time constant slower by at least one order of magnitude (τ_2 = 70–142 s). These SIFT response patterns for TI are similar to those resulting from step CSN inputs (59) except that neither a reflex component nor a fast integrator component (compare with the TE response) was evident.

Plasticity of ∫Phr. For both SI and SE CSN inputs, the response in ∫Phr paralleled those for TI but in opposite directions. The increase in ∫Phr in the steady state was significantly greater with SE than with SI CSN inputs (16.3 ± 5.9 vs. 8.8 ± 3.7%, $P < 0.05$).

Refined Functional Model of Carotid Chemoafferent Signaling

At first glance, the SIFT data (Fig. 7) seemed uninspiring, as both SI and SE CSN inputs elicited similar integrator and differentiator effects that proved to largely resemble those resulting from step CSN inputs (Fig. 5). Moreover, although the SE data seemed to verify the working model with phase-logic gating as delineated in Fig. 4*C*, the SI data did not. However, further application of the SIFT theory to the experimental data brought to light certain subtle features of carotid chemoafferent signaling that were obscured under step CSN or hypoxic inputs. These findings led to a refined functional model of carotid STP and STD

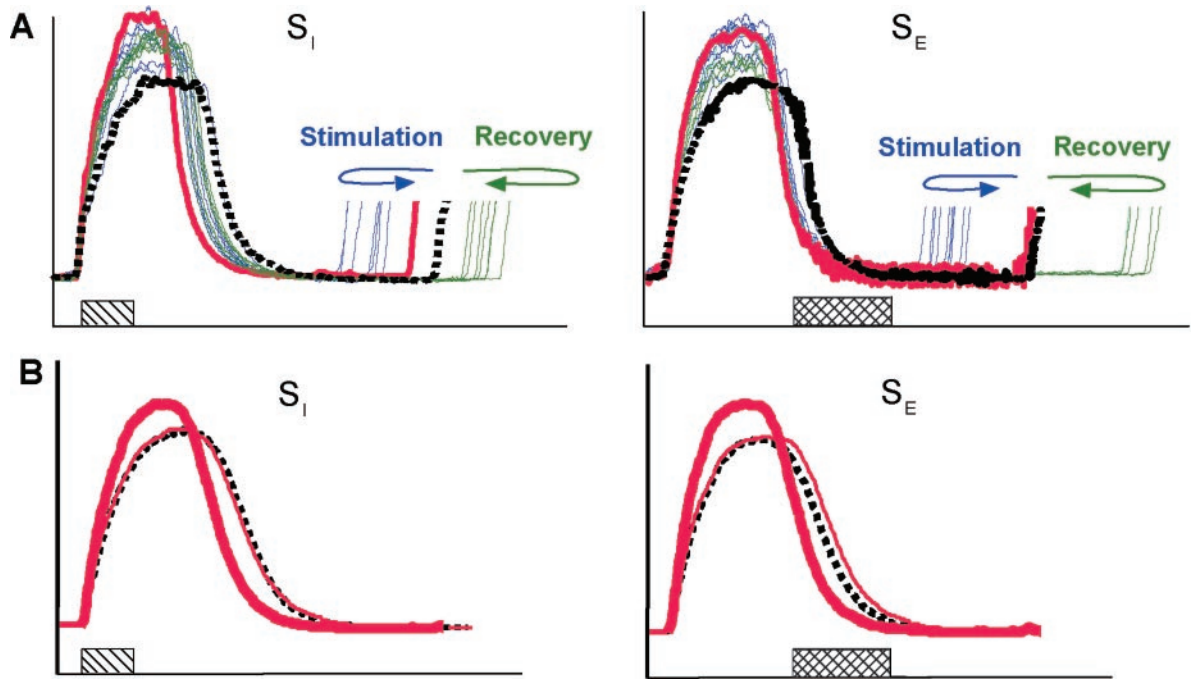

Fig. 6. Effects of strobe CSN pulse-train stimulation on the phrenic neurogram. Stimulus strobes (hatched and crosshatched bars, positioned relative to the bold red traces) were delivered either in SI (*left*) or SE (*right*). *A*: oscilloscopic displays of transient phrenic neurogram illustrating the time-dependent effects of SI and SE stimuli in 1 rat. Bold traces show the average integrated phrenic nerve (∫Phr) waveform during 1-min control period (bold, dashed black) and for the last 10 s of a 4-min stimulation period (bold red). Thin traces show the cycle-by-cycle plots of ∫Phr recorded over a 10-s time window at the beginning of stimulation (blue) and poststimulation (green). Arrows indicate corresponding bidirectional movements of expiratory-inspiratory off-switch under SI and SE. *B*: steady-state average phrenic waveforms ($n = 5$) are shown for the control period (dashed black) and for the last 10 s of the stimulated period either normalized in time and amplitude to the control waveshape (thin red) or nonnormalized (bold red). The averaged data show that the wave shape remains largely unchanged, except for increased amplitude and reduced TI.

(Fig. 8) that conforms with both step and strobe CSN inputs.[1]

Carotid chemoafferent pathways were phase-logic gated. Although the responses in TE, TI, and ∫Phr to SI and SE CSN inputs all exhibited integrator and differentiator patterns (Fig. 7), the integrator time constants for TE were significantly different from those for TI and ∫Phr ($P < 0.05$, Table 1), with no evidence of crossover either way (compare with Fig. 4). Therefore, it appears that all the carotid chemoafferent pathways were logically gated to either the E phase or I phase, as illustrated in Fig. 8. This observation supports the phase-logic gating hypothesis of the working model (Figs. 1*A* and 4) based on previous findings with step CSN inputs (Fig. 5).

Carotid "chemoreflex" shortened TE through a fast integrator gated to E phase. The working model assumed that CSN input shortened TE through an E-gated reflex pathway inhibitory to the E phase (Fig. 1*A*). The present results, however, showed that the response in TE at the onset/offset of the SE and SI CSN inputs (Fig. 7*A*) developed progressively over several breaths like an integrator, rather than abruptly within the first breath. This behavior was most striking under the SI CSN input, whereby any reflex modulation of TE would be suppressed by off-strobe filtering, and yet the integrator response in TE remained. These surprising revelations suggested that the carotid "chemoreflex" modulation of TE might be mediated indirectly by an E-gated secondary integrator rather than directly via a primary pathway (Fig. 8). The time constant of this occult integrator was extremely short (τ_1 = 1.5–3.0 s, Table 1) under strobe CSN inputs and perhaps even shorter under step CSN inputs (Fig. 5), making it difficult to discern within the resolution of a single respiratory cycle (~1.5 s in vagotomized rats).

Carotid STD lengthened TE through a slow-recovery integrator gated to E phase. In agreement with the working model (Fig. 1*A*), the SIFT data (Fig. 7*A*) demonstrated an E-promoting, E-gated integrator that had relatively fast induction and slow recovery (τ_2 = 6.5–7.8 s and 130–210 s, respectively), evidencing significant dynamic hysteresis (52). The response characteristic and the depression effect on the respiratory frequency suggest that this integrator may be associated with the pontine-mediated posthypoxic frequency depression response (6, 10). This pontine pathway for carotid STD (Fig. 8) is assumed to be connected in parallel with the E-inhibiting fast integrator described above because these integrators are seen to operate

[1] Animations of the model for expiratory and inspiratory strobe inputs are shown in the attached videoclips (http://jap.physiology.org/cgi/content/full/94/3/1213/DC1).

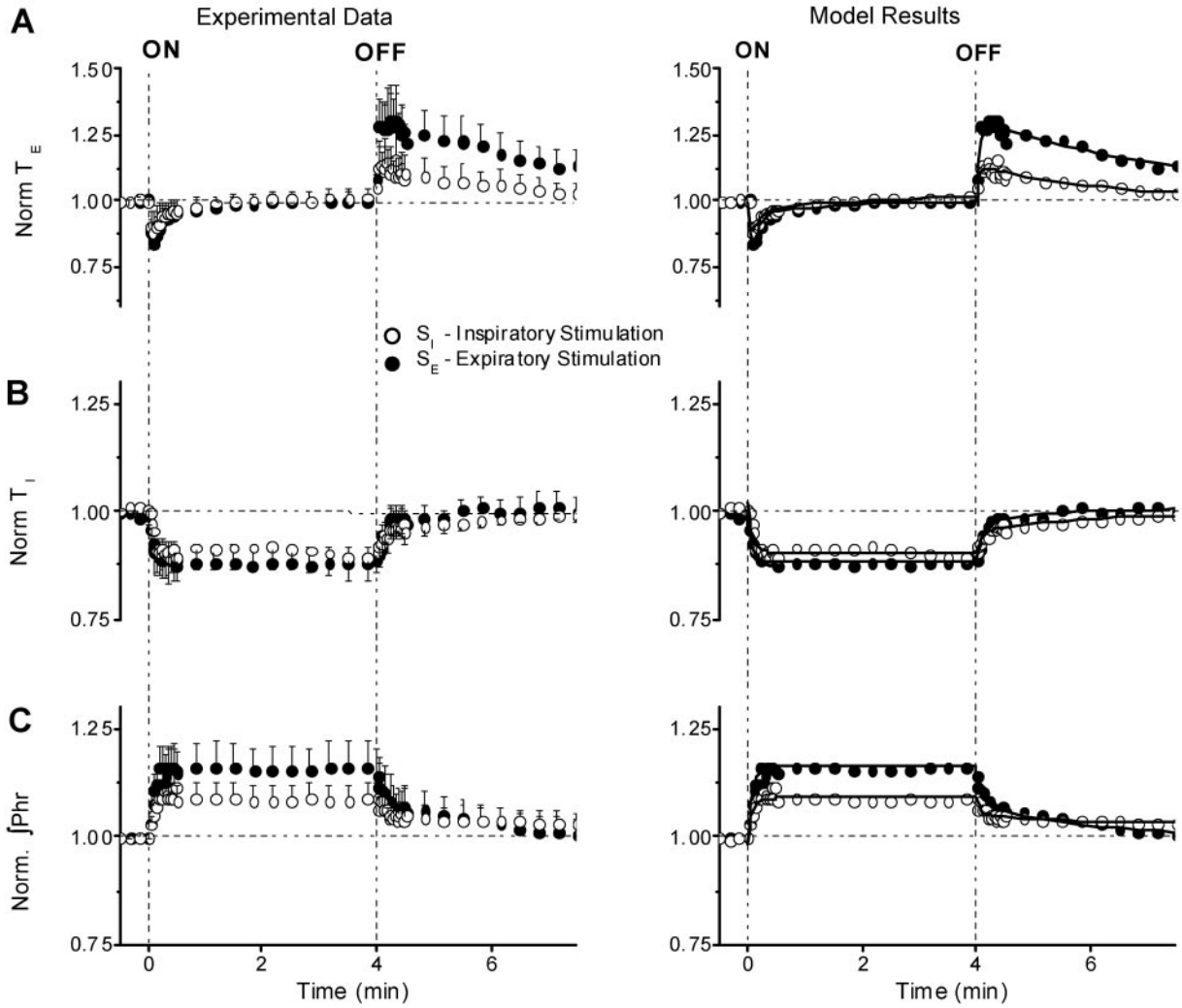

Fig. 7. Phase-contrast interference of respiratory rhythm by strobe CSN stimuli. Responses are expressed in terms of phrenic inter-burst interval (T_E; *A*), phrenic burst interval (T_I; *B*), and peak amplitude of ∫Phr (*C*). *Left*: data for CSN inputs (means ± SE, $n = 9$) were normalized (Norm) with respect to corresponding mean values during the control baseline periods. Baseline values for CSN were as follows: $T_E = 0.99 \pm 0.07$ s and $T_I = 0.39 \pm 0.02$ s. These values were similar for both S_I and S_E stimulation protocols. Vertical dashed lines indicate beginning and end of CSN stimulation. Note S_I and S_E inputs for CSN inputs resulted in similar integrator and differentiator characteristics in the 3 respiratory parameters. *Right*: multiexponential curve fits (solid lines) plotted against the mean experimental data during and after stimulation. Curve fit values were calculated using least-squares regression and compared with competing models using the *F* test ($P < 0.05$). Model parameters are reported in Table 1.

independently in widely differing timescales (especially in the recovery phase) and have opposite effects on T_E. Alternatively, these integrators could be connected in series, provided that there is a bypass for the slow integrator, which circumvents its low-pass filtering of the faster dynamics.

Lack of carotid chemoreflex in I phase under strobe CSN inputs. Remarkably, a reflex shortening of T_I typically seen during step CSN pulse-train stimulation in rats (Fig. 5) was absent with S_I CSN input (Fig. 7*B*). Because the S_I stimulus train during the I phase ended before I-E phase switching (see *Experimental Methods* and Fig. 6), it may be inferred that a CSN stimulus may elicit reflex shortening of T_I in rat provided it is applied late in the I phase. However, careful reexamination of the data in Fig. 5 revealed that this "chemoreflex" shortening and relengthening of T_I probably developed progressively in the first two breaths at the onset and offset of CSN stimulation, respectively, rather than abruptly within the first breath. Therefore, it seems that this apparent reflex response in T_I (if present) might also be mediated by a fast integrator in the I-related pathway as with the E-related pathway. This timing-dependent "chemoreflex" effect for T_I is depicted in the proposed functional model (Fig. 8) as a possible time-gated pathway to the I-neuron. A corresponding reflex pathway for Phr motor output is not included in Fig. 8, as such a reported reflex effect on ∫Phr in cats (16, 17, 79) was not indicated in the SIFT data

Table 1. *Estimated parameter values of multiexponential curve fitting*

Model Element	Parameter	S_E		S_I	
		On	Off	On	Off
T_E	y_0	1.004 ± 0.003	1.026 ± 0.046	1.010 ± 0.002	1.000 ± 0.012
Fast	A_1	0.341 ± 0.052	−0.332 ± 0.009	0.170 ± 0.010	−0.125 ± 0.005
Integrator	τ_1	2.111 ± 0.236	2.909 ± 0.171	1.560 ± 0.160	2.472 ± 0.243
STD	A_2	−0.276 ± 0.004	0.289 ± 0.043	−0.120 ± 0.005	0.131 ± 0.010
(Pons)	τ_2	6.547 ± 0.176	206.830 ± 54.301	7.780 ± 0.470	132.890 ± 25.484
STD/LTD	A_3	−0.061 ± 0.003	NS	−0.070 ± 0.004	NS
(NTS)	τ_3	79.501 ± 14.524	NS	65.780 ± 9.070	NS
T_I	y_0	0.882 ± 0.001	1.006 ± 0.003	0.904 ± 0.001	1.000 ± 0.001
STP	A_1	0.089 ± 0.002	−0.088 ± 0.004	0.114 ± 0.003	−0.051 ± 0.002
	τ_1	4.954 ± 0.151	6.784 ± 0.599	5.232 ± 0.280	6.882 ± 0.562
STP slow	A_2	NS*	−0.038 ± 0.003	NS*	−0.044 ± 0.001
	τ_2	NS*	70.966 ± 19.444	NS*	142.075 ± 8.509
∫Phr	y_0	1.166 ± 0.001	1.000 ± 0.001	1.091 ± 0.001	1.033 ± 0.002
STP	A_1	−0.173 ± 0.002	0.064 ± 0.004	−0.106 ± 0.002	0.039 ± 0.003
	τ_1	5.650 ± 0.180	4.602 ± 0.575	4.492 ± 0.178	4.118 ± 0.593
STP slow	A_2	NS*	0.079 ± 0.002	NS*	0.022 ± 0.002
	τ_2	NS*	106.570 ± 6.230	NS*	72.218 ± 22.664

Values are means ± SE. Model equation is as follows: $y = y_0 + A_1 \exp(-t/\tau_1) + A_2 \exp(-t/\tau_2) + A_3 \exp(-t/\tau_3)$. y, y_0, A_1, A_2, and A_3 are normalized magnitudes (dimensionless); τ_1, τ_2, are τ_3 are time constants (in s). ∫Phr, amplitude of integrated phrenic activity; T_E and T_I, expiratory and inspiratory duration; S_E and S_I, expiratory-strobe and inspiratory-strobe carotid sinus nerve stimulation; STD and STP, short-term depression and potentiation; LTD, long-term depression; NTS, nucleus tractus solitarius. NS, not significant by F test ($P > 0.1$). *Indeterminate due to cancellation of counteracting components (see text).

(Fig. 7) or in previous studies with step CSN input at relatively low-stimulation currents in rats (59).

Carotid STP shortened T_I through dual integrators gated to I phase. In agreement with the working model (Fig. 1*A*), both S_I and S_E CSN inputs revealed (Fig. 7*B*) an I-inhibiting, I-gated integrator with relatively fast induction and recovery time constants (τ_1 = 4–7 s for both). In addition, the SIFT data (Table 1) revealed a second integrator with a relatively slow recovery time constant (τ_2 = 70–140 s), although its induction dynamics was obscured by a counteracting monophasic integrator from the NTS (see below). These integrators are distinguished from those for T_E by their distinct onset/offset time constants. Again, these dual integrators are assumed to be connected in parallel (Fig. 8) in light of their independent actions over widely different timescales, although a series connection is also possible provided there is a bypass pathway for the slow integrator that circumvents its low-pass filtering of the faster dynamics.

Carotid STP augmented Phr activity through dual integrators gated to I phase. Similarly, the SIFT data suggested that the carotid STP of Phr motor output may be ascribed to I-gated dual integrators (Fig. 7*C* and Table 1). However, these dual integrators are distinguished from those for T_I in that they were Phr facilitating instead of I inhibiting. Furthermore, their response magnitudes were distinct for S_I and S_E CSN inputs, unlike the similar response magnitudes with T_I. Therefore, these integrators appear to have separate excitatory effects on I-PMN independent of the corresponding inhibitory effects on I-neuron (Fig. 8). Furthermore, because the S_I and S_E CSN inputs did not alter the Phr waveshape when normalized for T_I and amplitude of ∫Phr (Fig. 6), these carotid STP pathways to I-neuron and I-PMN appear to modulate mainly the timing and gain rather than the waveshape of inspiratory motor outflow.

Our data for Phr motor output do not exclude the possible contributions of long-term facilitation in respiratory oscillator neurons (43, 44), STP (39), or long-term facilitation (29) of the phrenic motor pathway and its phasic inhibition by bulbospinal inputs (47), although the stimulation protocols for the induction of these effects were different from those used in this study. It has been pointed out that such neural processing in the efferent pathway posterior to the respiratory oscillator is unlikely to affect the carotid STP for the T_I response (57). Further studies in the future are needed to identify the loci of carotid STP for the T_I and ∫Phr responses.

Synaptic STP/STD in NTS modulated carotid STP/STD. From the SIFT theory, synaptic STD/LTD in NTS may appear as a monophasic inverted integrator (Fig. 2*B*). Multiexponential analysis of the T_E response (Fig. 7 and Table 1) indeed identified such an inverted integrator, which emerged slowly during induction (τ_3 = 65–79 s) and was obscured during recovery. This monophasic inverted integrator for T_E was evident not only with S_E but also S_I CSN inputs, suggesting that the off-strobe filtering effect of the NTS integrator might be obscured by subsequent integration in the secondary pathways (Fig. 2*B*).

Multiexponential analysis of the T_I and ∫Phr data (Table 1) showed that the slow inspiratory STP integrators had a similar time constant (τ_2 = 70–140 s) as the NTS integrator identified above but had normal (noninverting) polarity. Consequently, although the slow STP integrator could be identified during the recovery period, neither it nor the NTS integrator was identifiable during the induction period (Table 1) as their effects collided and annihilated one another.

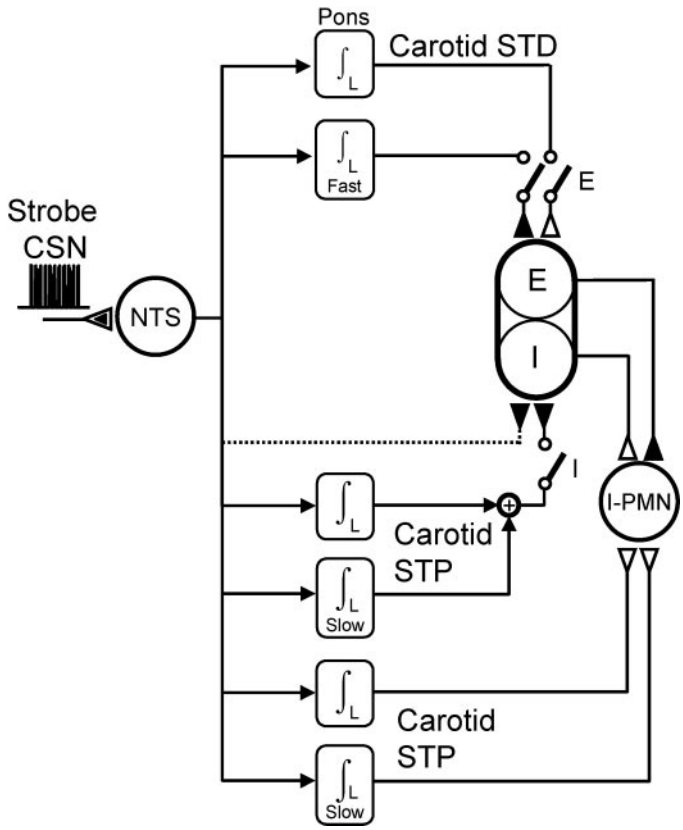

Fig. 8. Functional model of carotid chemoafferent signaling compatible with both strobe CSN and step CSN data. Conventions are as in Fig. 1*A*. Animations of the model for expiratory and inspiratory strobe inputs are shown in the attached videoclips (http://jap.physiology.org/cgi/content/full/94/3/1213/DC1). All pathways are phase-logic gated, as indicated by the switches. The carotid STD component shown to promote E phase likely resides in the pons (6), whereas the other pathway locales remain uncertain. Pathways terminating on the respiratory oscillator could have opposite (excitatory vs. inhibitory) polarities if they project to the opposite side of the oscillator (E-neuron instead of I-neuron and vice versa) or if they contain inverted integrators instead. Parallel integrators are functionally equivalent to serial integrators in cascade with a bypass pathway for the slower integrator. Dotted line indicates possible carotid "chemoreflex" pathway to I-neuron time gated to the late-I phase. See text.

These model predictions were verified by computer simulations (Fig. 9).

Model Simulations

Strobe CSN inputs. Figure 9*A* shows the model-simulated responses of the expiratory pathways to strobe CSN inputs. It can be seen that differential processing of the reflex-accommodation component of the NTS is provided by the excitatory-inhibitory actions of the dual integrators with differing response magnitudes (−0.28 vs. 0.34) and induction time constants (6.5 s vs. 2.1 s). However, the pontine integrator has a recovery time constant (207 s) that is more than 10 times slower than its induction, and such pronounced dynamic hysteresis makes it much less responsive to the subsequent STD/LTD component compared with the fast integrator (recovery time constant of ~2.9 s). As a result, the monophasic inverse integrator effect of the NTS is transmitted to the respiratory oscillator via the fast integrator virtually free of antagonism, adding to the differentiator effect of the expiratory pathways.

By contrast, the simulations in Fig. 9*B* show that the STD/LTD effect of the NTS during induction is annulled by the STP integrators in the inspiratory pathways, unlike the expiratory pathways. Specifically, the transmission of the inverse integrator component of the NTS via the slow integrator is dampened by the low-pass filtering action of the latter, and its transmission via the fast STP integrator is counterbalanced by the low-pass filtering of the reflex-accommodation component via the slow integrator. Similar effects were obtained in the simulations (not shown) of the responses of the STP integrators for I-PMN.

Step CSN inputs. The simulation results for step CSN inputs were qualitatively similar to those for strobe inputs (Fig. 9) except for differing integrator time constants (see Fig. 5 legend). The refined model simulated more closely the initial development and decay of the fast integrator responses (Fig. 5, *insets*) than the working model in Fig. 1A, which assumed that these responses were primarily reflex mediated. Thus the refined model extends the working model by accounting for both the fast and slow integrator effects in the carotid chemoafferent signaling pathways.

DISCUSSION

The SIFT data corroborate the hypothesis that carotid chemoafferent signaling via the NTS is dynamically filtered downstream by a parallel bank of integrators and differentiators in varying time and frequency scales, which are logically gated to the E and I half-cycles. The aptness of the proposed functional model is contingent on the soundness of the underlying theory and methodology, and its validation may shed light on the complex organization of carotid chemoafferent pathways for respiratory pattern generation.

Critique of Methodology

Modeling perspectives. Previous studies of respiratory control have focused on the identification of discrete cellular mechanisms in reduced or anatomically isolated preparations, with a view to accumulating a complete empirical basis piecemeal for ultimate bottom-up (cellular-to-system) integrative modeling. In contrast, the present study drew on largely top-down (system-to-cellular) integrative modeling based on experimental observations at the system level in order to discern the structural and functional organization of carotid chemoafferent pathways en bloc consistent with current understanding of related discrete mechanisms at the cellular level, with minimal assumptions about the structure of the respiratory oscillator. Both modeling approaches have advantages and disadvantages (84). At this stage, bottom-up modeling of carotid chemoafferent signaling is precluded by the current dearth of available information at both the cellular and

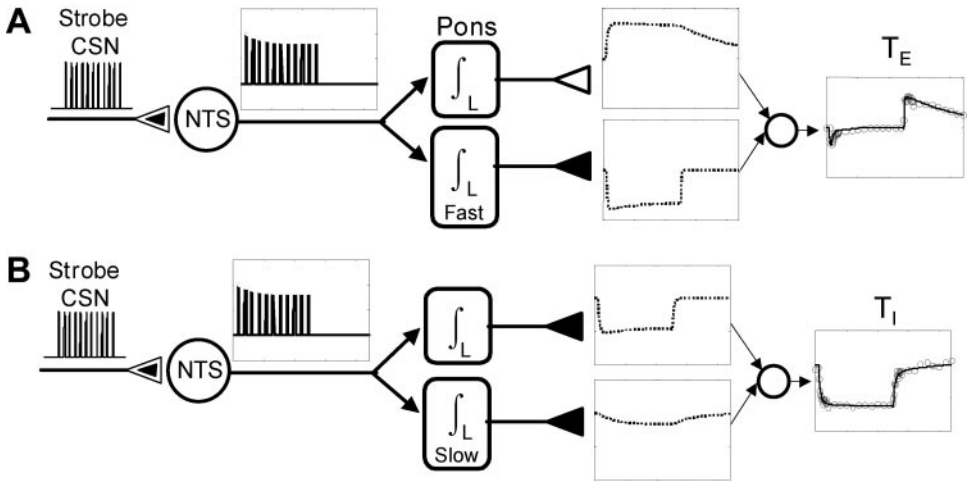

Fig. 9. Simulations of carotid chemoafferent signaling from NTS to the respiratory oscillator via expiratory pathways (*A*) and inspiratory pathways (*B*). Results for the pathways to I-PMN were similar to *B*. Simulations were based on the model shown in Fig. 8 with parameter values from Table 1, for the case of SE CSN activation. Simulations for SI CSN activation and continuous CSN activation were qualitatively similar to those in the SE case and are not shown. The phasic and STD/LTD responses in NTS are integrated continuously by dual integrators in secondary pathways, with the outputs (dotted lines in boxes) gated to either the respiratory E phase or I phase. The predicted response in the output (solid line) closely matched the mean experimental data (○) for TE and TI . Note the synaptic STD/LTD effect in NTS is preserved by the dual integrators in *A* and annihilated in *B*, depending on the integrator time constants and polarity of corresponding signaling pathways. See text.

system levels, which undersold the true complexity of the problem.

Armed with the SIFT theory, the present study revealed certain subtle features of carotid chemoafferent signaling and put in perspective the intricate interrelationships among various observed and hypothesized cellular mechanisms, which had largely eluded previous studies when viewed solely from bottom up. The resultant functional model unifies the reported synaptic modulations of NTS and pontine neurons, I- and E-related oscillator neurons and I-PMN. In addition, the model offers a methodical guidepost for the elucidation of other postulated cellular and network mechanisms that would make for bottom-up modeling in the future, with full validation of the underlying hypotheses only when bottom-up meets top-down (32, 50, 84).

SIFT as a probe for complex neural systems. Neural integrator, differentiator, and logic gating are novel physiological paradigms, and their elucidation calls for new experimental and theoretical methodologies. The intricate characteristics of these elemental processes and their manifold connectivity in a spatiotemporally extended network rendered carotid chemoafferent signaling with such complexity that defied experimental exploration with conventionally physiological, anatomic, and imaging approaches. Indeed, the seemingly mundane response characteristics under strobe CSN inputs (Fig. 7) belied the underlying peculiarities, which became transparent only under the magnifying glass of SIFT. In essence, SIFT helps to sift the data for insights beyond their face values (82). Without delving into its profound theoretical underpinning, the power of SIFT is due to two well-known techniques in phase-contrast imaging: stroboscopy (autogating effect) and interferometry (rhythmic interference effect). Systematic application of these basic principles to the SIFT data made it possible to noninvasively dissect the various reflex, memory, and gating effects of the carotid chemoafferent pathways and logically piece the jigsaw together, revealing their inner workings component-by-component and their overall architecture all at once.

In a recent study (82), the SIFT approach has been applied to reconstruct the central pathways mediating the vagal inputs from pulmonary slowly adapting stretch receptors. The results suggest a primary ungated excitatory pathway to the E neuron that mediates the classic Hering-Breuer reflex prolongation of TE and shortening of TI with corresponding habituation effects, together with a secondary E-gated pathway that mediates the desensitization of the Hering-Breuer reflex. These model predictions based on SIFT theory are confirmed by experimental evidence of a primary excitatory pathway mediating the Hering-Breuer reflex (19, 24) and a pontine pathway mediating its desensitization (75). The excellent agreement between experimental observations and model predictions provided a validation of the SIFT approach.

Validity of CSN stimulation. Pursuant to the SIFT theory, we used electrical CSN stimulation instead of natural stimuli to activate carotid chemoafferents in specific phases of the respiratory rhythm in an all-or-none fashion. The possible influence of baroreceptive CSN fibers may be discounted for several reasons. First, pressor responses are negligible with the relatively low-stimulation currents being used (49, 59). Second, it has been shown that carotid baroreceptor stimuli (13, 70) or aortic nerve stimulation (2, 23) have only relatively minor and disparate (inhibitory) effects on respiration compared with carotid chemoreceptor

stimuli or CSN stimulation. Third, both strobe and step CSN inputs (58, 59, 79) elicited similar respiratory responses as with natural stimuli (6, 23), consistent with carotid chemoafferent activation. It should be noted, however, that CSN stimulation reveals only the acute effects in central pathways and not any plasticity that might develop at the carotid chemoreceptors level (62) or over a longer term of hours and days (34, 61).

Organizing and Operating Principles of Carotid Chemoafferent Pathways

The proposed functional model (Fig. 8) suggests several possible organizing and operating principles of carotid chemoafferent signaling that are useful in understanding the underlying mechanism.

Dynamic signal conditioning. An interesting organizing principle demonstrated in the proposed model is that NTS signaling to the respiratory oscillator may be mediated indirectly by a bank of integrators via secondary pathways, with little or no direct reflex neurotransmission via primary pathways. Surprisingly, the carotid chemoreflex shortening of T_E (and probably also T_I) proved to be mediated by an occult fast integrator with tonic secondary excitation. Because of their high responsiveness, these fast integrators could be saturated rapidly within a normal respiratory cycle by a sustained strong stimulus, thus contributing to their elusiveness. In the present study, this occult integrator for T_E was discerned unambiguously with the use of strobe pulse-train stimulations at moderate intensities.

Because the integrators in the NTS and secondary pathways all have time constants in the order of one or two breaths or more, it appears that their function is to preferentially transmit sustained or slow increases or decreases in carotid chemoafferent feedback while filtering out extraneous within-breath variability. Additionally, these integrators may also act as accumulators that provide temporal buffering for the respiratory-related oscillations of carotid chemoreceptor feedback (3, 8, 18), allowing magnitude but not timing information of the CSN signal to be transmitted to the respiratory oscillator. This notion is supported by the presently observed similarity of the respiratory responses to S_I, S_E and tonic CSN inputs, indicating that the specific timing and phase of a CSN input within a respiratory cycle are relatively unimportant.

Logic gating. Another important organizing principle embodied by the proposed model is that the carotid chemoafferent pathways may be phase-locked to the respiratory rhythm. Functionally, such phase-locked behavior works like a logic gate or temporal filter, passing or suppressing neural traffic at selected time intervals. This fundamental organizing principle implies that carotid chemoafferent traffic may be regulated centrally in a highly orderly stop-and-go manner, much like the traffic lights at a crossroads. The advantages of such phase-logic gating or temporal filtering are obvious. Ungated tonic inputs to the E and I neurons are bound to elicit counteracting crossover responses in T_E and T_I, thus compromising their net effects on the respiratory frequency. Logic gating allows the E and I phase to be regulated independently by carotid chemoafferent feedback in a manner that is tailored to each phase.

The present findings extend early propositions of such phase-dependent gating in the chemoreflex loop (3, 18, 25) by demonstrating that carotid chemoafferent inputs are mediated by multiple integrator pathways with varying polarities and response dynamics, each of which is logically gated to the E or I phase. Our results showed that the effects of gating are highly complex in both spatial and temporal domains, such that stimuli delivered in one phase could affect not only the current phase but also the next phase through memory gated to that phase. This indirect action may occur rapidly in the E phase via a fast integrator with a short time constant (<3 s) but may take longer for the I phase. This explains why brief stimuli delivered acutely during an expiration failed to elicit any discernible effects in the next inspiration (4, 13), since repetitive stimulation might be needed to overcome the relatively slow dynamics of carotid STP of inspiratory activity.

In theory, phase-logic gating could also occur within the respiratory oscillator. For example, if the E-to-I branch of the reciprocal inhibition pathways is strengthened by carotid chemoreceptor activation, then the E phase would be lengthened without affecting the I phase. However, there is presently little evidence of such activity-dependent plasticity in the VRG. Because the induction of carotid STP and STD are dependent on NMDA receptors that regulate excitatory synaptic transmission (7, 58, 59), they are unlikely to result from plasticity of inhibitory connections. Furthermore, because any synaptic modifications within the respiratory oscillator must be preceded by changes in the activity of the respiratory neurons, the lack of any reflex response in T_I and T_E under strobe CSN inputs suggests that the integrator and gating effects are ascribable at least in part to the carotid chemoafferent pathways.

In contrast to phase-logic gating, previous studies have emphasized the importance of precise, within-phase timing of carotid chemoafferent inputs on respiration (15–17, 27, 35, 36, 63). Specifically, CSN stimuli were found to reflexly facilitate I or E activity in cats, provided that they were delivered in the later half of the corresponding phase. Stimuli during early I reflexly shortened that inspiration, whereas late stimuli prolonged it. Conversely, stimuli given in midexpiration reflexly prolonged that expiration, but late stimuli shortened it. In a previous study in dogs (26), phasic electrical CSN stimulation throughout the I or E phase paradoxically prolonged T_I. The seemingly conflicting observations in these early studies are confounded by the variable phase resetting patterns that could result from phasic CSN stimuli delivered near I-E or E-I phase switching (49).

In the present study in rats, we employed an experimental design that ensured that the S_I and S_E stimuli did not encroach on the E-I and I-E phase-switching

periods. The absence of stimulus-induced artifacts in respiratory phase switching is confirmed by the observation that the SI and SE CSN inputs produced similar effects on the respiratory rhythm, which also resembled those resulting from step CSN inputs. However, our results do not rule out the possible occurrence of temporal gating beyond the SI and SE time intervals, e.g., during the early postinspiratory stage of expiration. Also, a fast-integrator reflex pathway to the I-neuron gated to late-I intervals (Fig. 8) may be inferred by comparison of the observed effects of the SI CSN input and those of step CSN inputs (Fig. 5), although direct evidence of such a within-phase gating effect is lacking.

Parallel segregated processing. The carotid chemoafferent pathways appear to be organized in a parallel and segregated fashion in two respects. First, these pathways are segregated by their gating to distinct phases of the respiratory rhythm. Second, within each respiratory phase, there are dual integrators acting in parallel. Such parallel and segregated neural architecture allows multiple neural pathways to operate independently of one another with minimum cross talk (56). In contrast, in a series configuration, the response bandwidth would be necessarily limited by the integrator with the slowest dynamics unless it has a bypass pathway, which is inherent in homosynaptic or heterosynaptic forms of neural integrator (Fig. 1, *B* and *C*). For example, the relatively slow (homosynaptic) STD/LTD integrator in NTS is not limiting to the succeeding secondary integrators because it is secondary to direct reflex neurotransmission in NTS. Thus, functionally, it is as though the STD/LTD integrator in NTS acted in parallel with the secondary integrators even though structurally they are connected in series. In any event, some degree of segregation and parallelism seems necessary so that different integral-differential processing modes may operate independently of one another in multiple phase-specific spatial domains over a wide range of timescales.

Multivariate feedback compensation. The stability of closed-loop respiratory control is influenced importantly by changes in the gain and phase delay of the carotid chemoreflex response (28). It has been generally assumed that the dynamics of carotid chemoreceptor feedback is characterized by a linear compartment with a fast time constant ascribed to the carotid chemoreceptors (1). The present study showed that carotid chemoreceptor feedback is modulated centrally by nonlinear neurodynamic and neurological processes specific to various respiratory timing and amplitude components. Specifically, the combination of secondary integrators with varying polarities, response speeds, and phase-logic gates allows parallel integral-differential processing of the carotid chemoafferent signal, with resultant differentiator (high-pass filtering) effects for the E phase and integrator (low-pass filtering) effects for the I phase in varying frequency bands. From engineering systems theory (45), a high-pass filter affords graded phase-advance (phase-lead) compensation, whereas a low-pass filter introduces graded phase-lag compensation of the feedback signal, which could be suitably tuned to maximize closed-loop stability. In the respiratory system, such dynamic compensations of the gain and phase of multivariate afferent feedbacks are further modified by the dynamic hysteresis, stimulus threshold, and saturation effects (52) as well as self-organized redundancy (80) that are characteristic of carotid chemoafferent pathways. Such complex time-frequency filtering of carotid chemoafferent traffic with inherent activity- and phase-dependent nonlinearities may exert profound influence on respiratory stability during hypoxia and sleep (52, 83) and could contribute to the dynamic optimization of respiratory pattern and maintenance of homeostasis in health and in disease states (50, 51, 53, 55).

We thank Dr. M. Siniaia for assistance with the animal experiments and Drs. J. Duffin, D. Paydarfar, and G. Song for valuable comments on the manuscript.

D. L. Young was supported by National Institute of Mental Health individual predoctoral fellowship MH-12697. This work was supported by National Heart, Lung, and Blood Institute Grants HL-60064 and HL-67966.

REFERENCES

1. **Bellville JW, Whipp BJ, Kaufman RD, Swanson GD, Aqleh KA, and Wiberg DM.** Central and peripheral chemoreflex loop gain in normal and carotid body-resected subjects. *J Appl Physiol* 46: 843–853, 1979.
2. **Biscoe TJ and Sampson SR.** An analysis of the inhibition of phrenic motoneurones which occurs on stimulation of some cranial nerve afferents. *J Physiol* 209: 375–393, 1970.
3. **Black AM and Torrance RW.** Respiratory oscillations in chemoreceptor discharge in the control of breathing. *Respir Physiol* 13: 221–237, 1971.
4. **Bowes G, Andrey SM, Kozar LF, and Phillipson EA.** Carotid chemoreceptor regulation of expiratory duration. *J Appl Physiol* 54: 1195–1201, 1983.
5. **Bowes G, Andrey SM, Kozar LF, and Phillipson EA.** Role of the carotid chemoreceptors in regulation of inspiratory onset. *J Appl Physiol* 52: 863–868, 1982.
6. **Coles SK and Dick TE.** Neurones in the ventrolateral pons are required for post-hypoxic frequency decline in rats. *J Physiol* 15: 79–94, 1996.
7. **Coles SK, Ernsberger P, and Dick TE.** A role for NMDA receptors in posthypoxic frequency decline in the rat. *Am J Physiol Regul Integr Comp Physiol* 274: R1546–R1555, 1998. [Corrigenda. *Am J Physiol Regul Integr Comp Physiol* 275, Sept. 1998, following table of contents.]
8. **Cross BA, Grant BJ, Guz A, Jones PW, Semple SJ, and Stidwill RP.** Dependence of phrenic motoneurone output on the oscillatory component of arterial blood gas composition. *J Physiol* 290: 163–184, 1979.
9. **Cunningham DJC, Robbins PA, and Wolff CB.** Integration of respiratory responses to changes in alveolar partial pressures of CO_2 and O_2 and in arterial pH. In: *Handbook of Physiology. The Respiratory System.* Bethesda, MD: Am. Physiol. Soc., 1986, sect. 3, vol. II, pt. 2, chapt. 15, p. 475–528.
10. **Dick TE and Coles SK.** Ventrolateral pons mediates short-term depression of respiratory frequency after brief hypoxia. *Respir Physiol* 121: 87–100, 2000.
11. **Dogas Z, Krolo M, Stuth EA, Tonkovic-Capin M, Hopp FA, McCrimmon DR, and Zuperku EJ.** Differential effects of $GABA_A$ receptor antagonists in the control of respiratory neuronal discharge patterns. *J Neurophysiol* 80: 2368–2377, 1998.
12. **Douglas WW and Ritchie JM.** Cardiovascular reflexes produced by electrical excitation of non-medullated afferents in the vagus, carotid sinus and aortic nerves. *J Physiol* 134: 167–178, 1956.

13. **Dove EL and Katona PG.** Respiratory effects of brief baroreceptor stimuli in the anesthetized dog. *J Appl Physiol* 59: 1258–1265, 1985.
14. **Duffin J, Tian GF, and Peever JH.** Functional synaptic connections among respiratory neurons. *Respir Physiol* 122: 237–246, 2000.
15. **Eldridge FL.** Expiratory effects of brief carotid sinus nerve and carotid body stimulations. *Respir Physiol* 26: 395–410, 1976.
16. **Eldridge FL.** The importance of timing on the respiratory effects of intermittent carotid body chemoreceptor stimulation. *J Physiol* 222: 319–333, 1972.
17. **Eldridge FL.** The importance of timing on the respiratory effects of intermittent carotid sinus nerve stimulation. *J Physiol* 222: 297–318, 1972.
18. **Eldridge FL and Millhorn DE.** Oscillation, gating, and memory in the respiratory control system. In: *Handbook of Physiology. The Respiratory System*. Bethesda, MD: Am. Physiol. Soc., 1986, sect. 3, vol. II, pt. 1, chapt. 3, p. 93–114.
19. **Ezure K.** Synaptic connections between medullary respiratory neurons and considerations on the genesis of respiratory rhythm. *Prog Neurobiol* 35: 429–450, 1990.
20. **Felder RB and Mifflin SW.** Modulation of carotid sinus afferent input to nucleus tractus solitarius by parabrachial nucleus stimulation. *Circ Res* 63: 35–49, 1988.
21. **Finley JC and Katz DM.** The central organization of carotid body afferent projections to the brainstem of the rat. *Brain Res* 572: 108–116, 1992.
22. **Grodins FS, Buell J, and Bart AJ.** Mathematical analysis and digital simulation of the respiratory control system. *J Appl Physiol* 22: 260–276, 1967.
23. **Hayashi F, Coles SK, Bach KB, Mitchell GS, and McCrimmon DR.** Time-dependent phrenic nerve responses to carotid afferent activation; intact vs. decerebellate rats. *Am J Physiol Regul Integr Comp Physiol* 265: R811–R819, 1993.
24. **Hayashi F, Coles SK, and McCrimmon DR.** Respiratory neurons mediating the Breuer-Hering reflex prolongation of expiration in rat. *J Neurosci* 16: 6526–36, 1996.
25. **Hildebrandt JR.** Gating: a mechanism for selective receptivity in the respiratory center. *Fed Proc* 36: 2381–2385, 1977.
26. **Hopp FA, Seagard JL, Bajic J, and Zuperku EJ.** Respiratory responses to aortic and carotid chemoreceptor activation in the dog. *J Appl Physiol* 70: 2539–2550, 1991.
27. **Howard P, Bromberger-Barnea B, Fitzgerald RS, and Bane HN.** Ventilatory responses to peripheral nerve stimulation at different times in the respiratory cycle. *Respir Physiol* 7: 389–398, 1969.
28. **Khoo MC, Kronauer RE, and Strohl KP.** Factors inducing periodic breathing in humans: a general model. *J Appl Physiol* 53: 644–659, 1982.
29. **Kinkead R, Zhan WZ, Prakash YS, Bach KB, Sieck GC, and Mitchell GS.** Cervical dorsal rhizotomy enhances serotonergic innervation of phrenic motoneurons and serotonin-dependent long-term facilitation of respiratory motor output in rats. *J Neurosci* 18: 8436–8443, 1998.
30. **Krolo M, Stuth EA, Tonkovic-Capin M, Hopp FA, McCrimmon DR, and Zuperku EJ.** Relative magnitude of tonic and phasic synaptic excitation of medullary inspiratory neurons in dogs. *Am J Physiol Regul Integr Comp Physiol* 279: R639–R649, 2000.
31. **Lawson EE, Richter DW, Ballantyne D, and Lalley PM.** Peripheral chemoreceptor inputs to medullary inspiratory and postinspiratory neurons of cats. *Pflügers Arch* 414: 523–533, 1989.
32. **Lisberger SG and Nusbaum MP.** Motor systems: understanding motor circuits: where bottom-up meets top-down. *Curr Opin Neurobiol* 10: 673–675, 2000.
33. **Liu Z, Chen CY, and Bonham AC.** Frequency limits on aortic baroreceptor input to nucleus tractus solitarii. *Am J Physiol Heart Circ Physiol* 278: H577–H585, 2000.
34. **Mahamed S and Duffin J.** Repeated hypoxic exposures change respiratory chemoreflex control in humans. *J Physiol* 534: 595–603, 2001.
35. **Marek W and Prabhakar NR.** Electrical stimulation of arterial and central chemosensory afferents at different times in the respiratory cycle of the cat. II. Responses of respiratory muscles and their motor nerves. *Pflügers Arch* 403: 422–428, 1985.
36. **Marek W, Prabhakar NR, and Loeschcke HH.** Electrical stimulation of arterial and central chemosensory afferents at different times in the respiratory cycle of the cat. I. Ventilatory responses. *Pflügers Arch* 403: 414–421, 1985.
37. **Matsugu M, Duffin J, and Poon CS.** Entrainment, instability, quasi-periodicity, and chaos in a compound neural oscillator. *J Comput Neurosci* 5: 31–51, 1998.
38. **McCormick DA.** Brain calculus: neural integration and persistent activity. *Nat Neurosci* 4: 113–114, 2001.
39. **McCrimmon DR, Zuperku EJ, Hayashi F, Dogas Z, Hinrichsen CFL, Stuth EA, Tonkovic-Capin M, Krolo M, and Hopp FA.** Modulation of the synaptic drive to respiratory premotor and motor neurons. *Respir Physiol* 110: 161–176, 1997.
40. **Mifflin SW and Felder RB.** Synaptic mechanisms regulating cardiovascular afferent signals to solitary tract nucleus. *Am J Physiol Heart Circ Physiol* 259: H653–H661, 1990.
41. **Miles R.** Frequency dependence of synaptic transmission in nucleus of the solitary tract in vitro. *J Neurophysiol* 55: 1076–1090, 1986.
42. **Morris KF, Arata A, Shannon R, and Lindsey BG.** Inspiratory drive and phase duration during carotid chemoreceptor stimulation in the cat: medullary neurone correlations. *J Physiol* 491: 241–259, 1996.
43. **Morris KF, Baekey DM, Shannon R, and Lindsey BG.** Respiratory neural activity during long-term facilitation. *Respir Physiol* 121: 119–133, 2000.
44. **Morris KF, Shannon R, and Lindsey BG.** Changes in cat medullary neurone firing rates and synchrony following induction of respiratory long-term facilitation. *J Physiol* 532: 483–497, 2001.
45. **Ogata K.** *Modern Control Engineering*. Englewood Cliffs, NJ: Prentice Hall, 1997.
46. **Owens NC and Verberne AJ.** An electrophysiological study of the medial prefrontal cortical projection to the nucleus of the solitary tract in rat. *Exp Brain Res* 110: 55–61, 1996.
47. **Parkis MA, Dong X, Feldman JL, and Funk GD.** Concurrent inhibition and excitation of phrenic motoneurons during inspiration: phase-specific control of excitability. *J Neurosci* 19: 2368–2380, 1999.
48. **Paton JF, Li YW, and Kasparov S.** Reflex response and convergence of pharyngoesophageal and peripheral chemoreceptors in the nucleus of the solitary tract. *Neuroscience* 93: 143–154, 1999.
49. **Paydarfar D, Eldridge FL, and Paydarfar JA.** Phase resetting of the respiratory oscillator by carotid sinus nerve stimulation in cats. *J Physiol* 506: 515–528, 1998.
50. **Poon CS.** Introduction: optimization hypothesis in the control of breathing. In: *Control of Breathing and its Modeling Perspective*, edited by Honda Y, Miyamoto Y, Konno K, and Widdicombe J. New York: Plenum, 1992, p. 371–384.
51. **Poon CS.** Self-tuning optimal regulation of respiratory motor output by Hebbian covariance learning. *Neural Networks* 9: 1367–1383, 1996.
52. **Poon CS.** Synaptic plasticity and respiratory control. In: *Bioengineering Approaches to Pulmonary Physiology and Medicine*, edited by Khoo MCK. Los Angeles, CA: Plenum, 1996, p. 93–113.
53. **Poon CS.** Ventilatory control in hypercapnia and exercise: optimization hypothesis. *J Appl Physiol* 62: 2447–2459, 1987.
54. **Poon CS and Bantikyan A.** Polyamines facilitate NMDAR-dependent synaptic long-term potentiation in nucleus tractus solitarius (Abstract). *Soc Neurosci Abstr* 347.7, 2002.
55. **Poon CS, Lin SL, and Knudson OB.** Optimization character of inspiratory neural drive. *J Appl Physiol* 72: 2005–2017, 1992.
56. **Poon CS and Shah JV.** Hebbian learning in parallel and modular memories. *Biol Cybern* 78: 79–86, 1998.
57. **Poon CS and Siniaia MS.** Plasticity of cardiorespiratory neural processing: classification and computational functions. *Respir Physiol* 122: 83–109, 2000.
58. **Poon CS, Siniaia MS, and Young DL.** High-pass filtering of carotid-vagal influences on expiration in rat: role of NMDA receptors. *Neurosci Lett* 284: 5–8, 2000.

59. **Poon CS, Siniaia MS, Young DL, and Eldridge FL.** Short-term potentiation of carotid chemoreflexes: an NMDA-dependent neural integrator. *Neuroreport* 10: 2261–2265, 1999.
60. **Poon CS, Zhou Z, and Champagnat J.** NMDA receptor activity in utero averts respiratory depression and anomalous LTD in newborn mice. *J Neurosci* 20: 1–6, 2000.
61. **Powell FL, Milsom WK, and Mitchell GS.** Time domains of the hypoxic ventilatory response. *Respir Physiol* 112: 123–134, 1998.
62. **Prabhakar NR.** Oxygen sensing during intermittent hypoxia: cellular and molecular mechanisms. *J Appl Physiol* 90: 1985–1994, 2001.
63. **Remmers JE, Richter DW, Ballantyne D, Bainton CR, and Klein JP.** Reflex prolongation of stage I of expiration. *Pflügers Arch* 407: 190–198, 1986.
64. **Rosen MJ.** A theoretical neural integrator. *IEEE Trans Biomed Eng* 19: 362–367, 1972.
65. **Rybak IA, Paton JF, and Schwaber JS.** Modeling neural mechanisms for genesis of respiratory rhythm and pattern. I. Models of respiratory neurons. *J Neurophysiol* 77: 1994–2006, 1997.
66. **Rybak IA, Paton JF, and Schwaber JS.** Modeling neural mechanisms for genesis of respiratory rhythm and pattern. II. Network models of the central respiratory pattern generator. *J Neurophysiol* 77: 2007–2026, 1997.
67. **Rybak IA, Paton JF, and Schwaber JS.** Modeling neural mechanisms for genesis of respiratory rhythm and pattern. III. Comparison of model performances during afferent nerve stimulation. *J Neurophysiol* 77: 2027–2039, 1997.
68. **Saha S, Batten TF, and Henderson Z.** A GABAergic projection from the central nucleus of the amygdala to the nucleus of the solitary tract: a combined anterograde tracing and electron microscopic immunohistochemical study. *Neuroscience* 99: 613–626, 2000.
69. **Sapru HN.** Carotid chemoreflex. Neural pathways and transmitters. *Adv Exp Med Biol* 410: 357–364, 1996.
70. **Saupe KW, Smith CA, Henderson KS, and Dempsey JA.** Respiratory and cardiovascular responses to increased and decreased carotid sinus pressure in sleeping dogs. *J Appl Physiol* 78: 1688–1698, 1995.
71. **Sears TA.** Spinal integration and rhythm generation in breathing. *Bull Eur Physiopath Respir* 20: 399–401, 1984.
72. **Shannon R.** Respiratory frequency control during hypercapnia in vagotomized, anesthetized cats. *Respir Physiol* 27: 357–367, 1976.
73. **Shen L.** Neural integration by short term potentiation. *Biol Cybern* 61: 319–325, 1989.
74. **Silva-Carvalho L, Dawid-Milner MS, Goldsmith GE, and Spyer KM.** Hypothalamic modulation of the arterial chemoreceptor reflex in the anaesthetized cat: role of the nucleus tractus solitarii. *J Physiol* 487: 751–760, 1995.
75. **Siniaia MS, Young DL, and Poon CS.** Habituation and desensitization of the Hering-Breuer reflex in rat. *J Physiol* 523: 479–491, 2000.
76. **Skinner FK, Turrigiano GG, and Marder E.** Frequency and burst duration in oscillating neurons and two-cell networks. *Biol Cybern* 69: 375–383, 1993.
77. **Smith JC, Butera RJ, Koshiya N, Del Negro C, Wilson CG, and Johnson SM.** Respiratory rhythm generation in neonatal and adult mammals: the hybrid pacemaker-network model. *Respir Physiol* 122: 131–147, 2000.
78. **Van der Kooy D, Koda LY, McGinty JF, Gerfen CR, and Bloom FE.** The organization of projections from the cortex, amygdala, and hypothalamus to the nucleus of the solitary tract in rat. *J Comp Neurol* 224: 1–24, 1984.
79. **Wagner P and Eldridge F.** Development of short-term potentiation of respiration. *Respir Physiol* 83: 129–139, 1991.
80. **Ward SA and Poon CS.** Beyond chemoreflex: plasticity, redundancy and self-organization in respiratory control. In: *Frontiers in Modeling and Control of Breathing: Integration at Molecular, Cellular and Systems Levels*, edited by Poon C-S and Kazemi H. New York: Kluwer Academic/Plenum, 2001, p. 267–272.
81. **Whitehead MC, Bergula A, and Holliday K.** Forebrain projections to the rostral nucleus of the solitary tract in the hamster. *J Comp Neurol* 422: 429–447, 2000.
82. **Young DL.** Neural adaptive mechanisms in respiratory regulation: theory and experiments. In: *Mechanical Engineering*. Cambridge, MA: Massachusetts Institute of Technology, 2002.
83. **Young DL and Poon CS.** Models of adaptive respiratory control and their clinical implications. *Jap J Med Electronics Biol Engineering* 16: 12–19, 2002.
84. **Young DL and Poon CS.** Soul searching and heart throbbing for biological modeling. *Behav Brain Sci* 24: 1080–1081, 2002.
85. **Zhou Z, Champagnat J, and Poon CS.** Phasic and long-term depression in brainstem nucleus tractus solitarius neurons: differing roles of AMPA receptor desensitization. *J Neurosci* 17: 5349–5356, 1997.
86. **Zhou Z and Poon CS.** Field potential analysis of synaptic transmission in spiking neurons in a sparse and irregular neuronal structure in vitro. *J Neurosci Methods* 94: 193–203, 2000.